Clinical Cancer Research

The Proteome of Prostate Cancer Bone Metastasis Reveals Heterogeneity with Prognostic Implications

Diego Iglesias-Gato[1,2], Elin Thysell[3], Stefka Tyanova[4], Sead Crnalic[5], Alberto Santos[6], Thiago S. Lima[1,2], Tamar Geiger[7], Jürgen Cox[4], Anders Widmark[8], Anders Bergh[3], Matthias Mann[4,6], Amilcar Flores-Morales[1,2], and Pernilla Wikström[3]

Abstract

Purpose: Bone is the most predominant site of distant metastasis in prostate cancer, and patients have limited therapeutic options at this stage.

Experimental Design: We performed a system-wide quantitative proteomic analysis of bone metastatic prostate tumors from 22 patients operated to relieve spinal cord compression. At the time of surgery, most patients had relapsed after androgen-deprivation therapy, while 5 were previously untreated. An extended cohort of prostate cancer bone metastases ($n = 65$) was used for immunohistochemical validation.

Results: On average, 5,067 proteins were identified and quantified per tumor. Compared with primary tumors ($n = 26$), bone metastases were more heterogeneous and showed increased levels of proteins involved in cell-cycle progression, DNA damage response, RNA processing, and fatty acid β-oxidation; and reduced levels of proteins were related to cell adhesion and carbohydrate metabolism. Within bone metastases, we identified two phenotypic subgroups: BM1, expressing higher levels of AR canonical targets, and mitochondrial and Golgi apparatus resident proteins; and BM2, with increased expression of proliferation and DNA repair–related proteins. The two subgroups, validated by the inverse correlation between MCM3 and prostate specific antigen immunoreactivity, were related to disease prognosis, suggesting that this molecular heterogeneity should be considered when developing personalized therapies.

Conclusions: This work is the first system-wide quantitative characterization of the proteome of prostate cancer bone metastases and a valuable resource for understanding the etiology of prostate cancer progression. *Clin Cancer Res; 24(21); 5433–44. ©2018 AACR.*

Introduction

Mortality in prostate cancer is strongly associated with development of bone metastatic disease (1, 2). Prostate cancer metastases are generally treated with androgen ablation (3). This therapy is initially effective, but most patients relapse to a castration-resistant stage. Despite recent treatment developments for patients with castration-resistant bone metastases (mCRPC), their prognosis remains poor with a median survival below 2 years (4). This is in contrast to patients harboring prostate confined tumors, who have a 10-year cancer-specific survival rate above 90%, even for patients managed by observation protocols (5, 6). Why metastatic tumors have a more aggressive behavior than localized tumors is not fully understood. Recent genetic studies have identified only a modest increase in the number and frequency of genetic aberrations in lethal, therapy-resistant metastatic cancer as compared with localized tumors (e.g., *TP53*, *PTEN*, *FOXA1*, and *PI3KCA*) with the exception of androgen receptor (*AR*) amplifications, rearrangements, and mutations, seen almost exclusively in CRPC (7, 8). One possible explanation for these findings is that many of the low-frequency mutations occurring in individual tumors may confer growth advantages through the regulation of a set of core signaling pathways required for metastatic growth. For example, mutations in genes such as *FOXA1* or *MLL2*, with apparently unrelated functions, may influence tumor growth through a common signaling mechanism: the regulation of AR activity (9). Many of the alterations in protein signaling associated with metastatic progression have remained undiscovered, as only few studies have actually examined prostate bone metastases in depth at the proteome level (10).

Transcriptomics or genetic analysis provides a partial view of the signaling pathways driving tumor growth because of their limited capacity to predict concentration changes at the protein level or inform about status of protein-driven mechanisms

[1]Department of Drug Design and Pharmacology, Faculty of Health and Medical Sciences, University of Copenhagen, Copenhagen, Denmark. [2]The Danish Cancer Society, Copenhagen, Denmark. [3]Department of Medical Biosciences, Pathology, Umeå University, Umeå, Sweden. [4]Department of Proteomics and Signal Transduction, Max Planck Institute of Biochemistry, Martinsried, Germany. [5]Department of Surgical and Perioperative Sciences, Orthopaedics, Umeå University, Umeå, Sweden. [6]The Novo Nordisk Foundation Centre for Protein Research, Faculty of Health Sciences, University of Copenhagen, Copenhagen, Denmark. [7]Department of Human Molecular Genetics and Biochemistry, Sackler School of Medicine, Tel Aviv University, Tel Aviv, Israel. [8]Department of Radiation Sciences, Oncology, Umeå University, Umeå, Sweden.

Note: Supplementary data for this article are available at Clinical Cancer Research Online (http://clincancerres.aacrjournals.org/).

A. Flores-Morales and P. Wikström share senior authorship of this article.

Corresponding Author: Diego Iglesias-Gato, University of Copenhagen, Universitetsparken 2, Copenhagen 2100, Denmark. Phone: 4535330640; Fax: 4535325001; E-mail: diego.iglesias@sund.ku.dk

doi: 10.1158/1078-0432.CCR-18-1229

Translational Relevance

We performed a global quantification of the proteins expressed in prostate cancer bone metastatic tumors and found wide variation in their proliferative and metabolic features. This variability is related to disease prognosis and should be accounted for when stratifying patients into different treatments.

(11, 12). Quantitative proteomic analysis of tumor samples may have a large potential to unveil novel signaling mechanisms of clinical relevance. We have recently analyzed the proteome of primary prostate tumors and demonstrated the upregulation of various proteins involved in metabolic processes in malignant compared with nonmalignant tissue (13). Remarkably, we did not observe a general increase of proteins involved in cell-cycle progression or DNA synthesis, perhaps reflecting the low proliferative capacity of most localized prostate tumors.

The objective of this first-in-class study was to characterize prostate cancer bone metastases in depth at the protein level and, by integrating these results with the previously described proteomic profiles of localized prostate tumors (13), to describe the proteome evolution during prostate cancer progression. Furthermore, we aimed to identify putative targets for novel therapies of metastatic CRPC and also to explore whether subgroups of prostate cancer bone metastasis exist that could potentially guide therapy decisions. We used system-wide quantitative mass spectrometry–based proteomic analysis to describe the proteome of prostate cancer bone metastases, and we found a high degree of heterogeneity among the analyzed samples with at least two phenotypically distinct subgroups of bone metastases. We propose that these subgroups should be accounted for when designing novel therapeutic alternatives.

Materials and Methods

Cohort description

Bone metastasis samples were obtained from men with prostate cancer, who underwent surgery for metastatic spinal cord compression at Umeå University Hospital between 2003 and 2014. Metastasis biopsies were fixed in 4% buffered formalin and decalcified in 20% formic acid for 1 to 3 days, according to clinical routines, before being embedded in paraffin. Clinical characteristics of the explorative, proteomic cohort ($n = 22$) and the extended cohort used for IHC validation ($n = 65$) are described in Table 1. For some cases of the proteomic cohort ($n = 12$–14), there were also available diagnostic, primary tumor biopsies for IHC analysis. In summary, most patients were diagnosed with tumors considered as high risk due to extensive growth in the biopsies, poor differentiation (high GS) and with locally advanced or metastatic disease. In patients where prostate cancer was not diagnosed until it caused neurologic symptoms [patients without androgen-deprivation therapy (ADT) at metastasis surgery], the primary tumor was not biopsied. Most patients were directly treated with ADT and only 2 patients were treated with curative intent (Table 1). At relapse to castration, patients received second-line treatments as indicated (Table 1). The study was approved by the local ethic review board of Umeå University (Dnr 03-185, Dnr 04-026M, decision August 24, 2007, Dnr 2013-372-32M) and conducted following the principles of the Declaration of Helsinki. All participants gave written or verbal consent. Due to the acute situation, when bone metastasis surgery is performed in order to relieve spine symptoms and paresis, logistics do not always allow written consent and the local ethic review board therefore specifically approved verbal consent as well. Verbal consent is documented by the physician in the patient journal.

Proteomic analysis

The effects of formic acid-based decalcification in the proteomic analysis were evaluated in a separate set of samples. No obvious quantitative or qualitative protein alterations were observed (Supplementary Fig. S1A). Protein extracts were obtained from approximately 20 microtome sections of 10-μm thick 25- to 50-mm^2 tumor-enriched areas. Mass spectrometry–based proteomic analysis of the bone metastasis samples was performed as previously described using SuperSILAC spike-in standards for accurate quantification (ref. 13; and extended Materials and Methods). The proteomic pipeline is summarized in Supplementary Fig. S1B. Raw data files were uploaded to ProteomeXchange. Accession references for published primary tumors and nonmalignant adjacent tissue are PXD004159, PXD004132, PXD003636, PXD003615, PXD003515, PXD003452, and PXD003430 (13). Accession reference for metastatic samples is PXD009868.

Bioinformatic tools and statistics

Unsupervised hierarchical clustering of metastasis samples was performed based on Pearson correlation coefficients as distance metrics (Fig. 1E). Gene ontology (GO) classification and enrichment analysis was performed using DAVID (14), and results were graphically represented with Cytoscape (ref. 15; Figs. 2 and 3).

Metastatic subgroups were defined by the Pearson correlation coefficients of the SILAC ratios of each protein across the cohort with the average SILAC ratio of the minichromosome maintenance complex components (MCM2-7) of each individual tumor (Fig. 3A). Only proteins showing 2 of 3 of valid SILAC ratios were used in the analysis. SILAC ratios of proteins with significant correlation ($P < 0.05$) to the MCM complex were used for hierarchical clustering. DAVID (14) was used to analyze the GO enrichment of the proteins with significant, positive, or negative, correlation to the MCM. Protein–protein interactions of components of significantly enriched processes were plotted using Cytoscape (15) according to their String score (16; Fig. 3B). Comparison between gene-expression and protein profiles (Fig. 4A and B) was carried out using the Gene Set Enrichment Analysis (GSEA) software (17).

To estimate the relative amount of subcellular components per cell (Fig. 4D), the sum of the label-free quantification intensity (18) of all proteins described as components of the organelle of interest was divided by the sum of all the nucleosomal proteins quantified in a given tumor sample. Only proteins quantified in all the samples were used.

IHC

Tissue sections were deparaffinized in xylene and rehydrated through graded ethanol. IHC staining was performed using MCM3 (HPA004789, Atlas Antibodies, diluted 1:100) and prostate specific antigen (PSA; A0562, DAKO, diluted 1:1,000)

antibodies, the ultraView Universal DAB Detection kit (760-500) and the automatic VENTANA Benchmark Ultra system, according to the manufacturer's description (Roche Diagnostics). PSA was stained without tissue pretreatment and MCM3 by using the CCL2 standard method (VENTANA, Roche Diagnostics). Immunostained sections were mounted and imaged and evaluated by using the Pannoramic 250 FLASH scanner and the Pannoramic viewer 1.15.2 software (3D HISTECH). The fraction of MCM3 immunopositive tumor nuclei was evaluated by counting on average 188 cells (117-437) cells per sample. The PSA staining were quantified by scoring the intensity (0 = no staining, 1 = weak, 2 = moderate, and 3 = intense staining) and the percentage of stained tumor cells (1 = 1%–25%, 2 = 26%–50%, 3 = 51%–75%, and 4 = 76%–100%). A combined PSA immune-reactive score, ranging from 0 to 12, was calculated by multiplying intensity with distribution.

Results

Proteomic profiling of prostate cancer bone metastasis samples provides additional information to transcriptomic profiling

Formalin-fixed paraffin-embedded prostate cancer bone metastasis samples, resected from 22 patients (Table 1), were decalcified and analyzed by quantitative LC-MS/MS using a spiked-in standard derived from isotopically labeled prostate cancer cell lines, as previously described (ref. 13; Supplementary Fig. S1B and extended Materials and Methods). On average, 5,067 proteins per sample were identified showing valid ratios for a total of 7,663 proteins (Fig. 1A; Supplementary Table S1).

We previously obtained global transcriptomic profiles from 20 of these bone metastases (included in GEO data sets GSE29650 and GSE101607; refs. 19, 20). Similar to observations in other cancer types (12, 21), and recently reported for prostate cancer (22), we found a positive but limited correlation between variations in mRNA and changes in the corresponding protein expression across the samples analyzed. The mean Spearman ρ was 0.28 (−0.69 to 0.92), with 31% of those correlations being statistically significant ($P < 0.05$; Fig. 1B). Particularly, genes involved in mRNA translation, oxidative phosphorylation, and components of the ribosomes and proteasome exhibited low degree of mRNA–protein correlation, with some even showing significantly negative correlations (Fig. 1C). These results suggest that in prostate cancer, protein expression measurements are required to fully investigate the relevance of many pathways for which analysis of variations in RNA steady-state levels would lead to inaccurate conclusions. The discrepancies between RNA and protein expression should be taken into consideration at the time of experimental planning and data interpretation.

Table 1. Patient characteristics at prostate cancer diagnosis and at time for orthopedic surgery due to bone metastasis complications

	Proteomic cohort ($n = 22$)	Validation cohort ($n = 65$)
Age at diagnosis (y)	72 (63; 77)	69 (63; 75)
Age at metastasis surgery (y)	73 (65; 81)	71 (67; 78)
PSA at diagnosis (ng/mL)	110 (46; 990)	100 (42; 750)
PSA at metastasis surgery (ng/mL)	241 (41; 1,100)	260 (61; 830)
Follow-up after diagnosis (mo.)	38 (26; 69)	43 (25; 73)
Follow-up after first ADT (mo.)	38 (26; 64)	42 (25; 71)
Follow-up after metastasis surgery (mo.)	12 (2.4; 32)	10 (3.0; 24)
Gleason score at diagnosis		
7	4	17
8	6	17
9	5	13
Not available	7	18
Radical prostatectomy		
Yes	0	2
No	22	63
Previous ADT		
None	5	15
Short-term	1	
Long-term	16	50
Treatment for CRPC		
Bicalutamide	8	27
Chemotherapy	1	8
Ra223	1	6
Bisphosphonate	2	6
Radiation toward operation site	1	8

Median (25th and 75th percentiles).

Prostate cancer bone metastases are more heterogeneous than tumors restricted to the prostate gland

The use of the same super-SILAC spike-in standard for the analysis of bone metastases as for localized tumor tissue obtained from prostatectomy specimens (of independent patients; ref. 13) allowed us to compare these protein profiles, in order to obtain a global picture of prostate cancer progression at the proteome level. Protein expression profiles of localized tumors and bone metastases were significantly correlated (average Pearson correlation of ρ: 0.61, $P < 0.001$; Fig. 1D). However, the average correlation for protein profiles within the metastatic group (ρ: 0.64 ± 0.077) was lower than that of the localized tumors (ρ: 0.8 ± 0.037) and the benign prostate tissues (ρ: 0.83 ± 0.03; Fig. 1E), indicating a higher degree of expressional heterogeneity among bone metastases than prostatectomy samples. Accordingly, unsupervised hierarchical clustering based on Pearson correlation of all the samples retrieved two main clusters; one containing all but one metastatic tumor and the other, grouping the localized tumors and benign samples (Fig. 1E). This indicates major differences between localized and metastasized prostate cancer at the proteome level. Strikingly, protein profiles from treatment-naïve bone metastasis tumors (samples PC31–35) and one metastasis collected shortly after the beginning of the castration protocol (PC36) clustered together with CRPC metastases instead of with primary tumors.

Major cellular processes altered in the transition from localized prostate cancer to bone metastasis

In order to identify biological pathways involved in prostate cancer progression, we performed GO enrichment analysis of the proteins differentially expressed in bone metastases compared with primary tumors (Fig. 2). Proteins functionally related to cell-cycle progression, DNA replication, and DNA damage repair were significantly upregulated in the metastatic setting (Fig. 2A). Importantly, these alterations were not observed in localized prostate tumors when compared with neighboring control tissue (13), suggesting that increased proliferation rates are acquired at a later stage during prostate cancer progression. On the other hand, some of the changes observed already in localized tumors get exacerbated in the metastases, as is the case of reduced expression of proteins involved in cell adhesion and carbohydrate metabolism (Fig. 2B) as well as increased expression of proteins involved

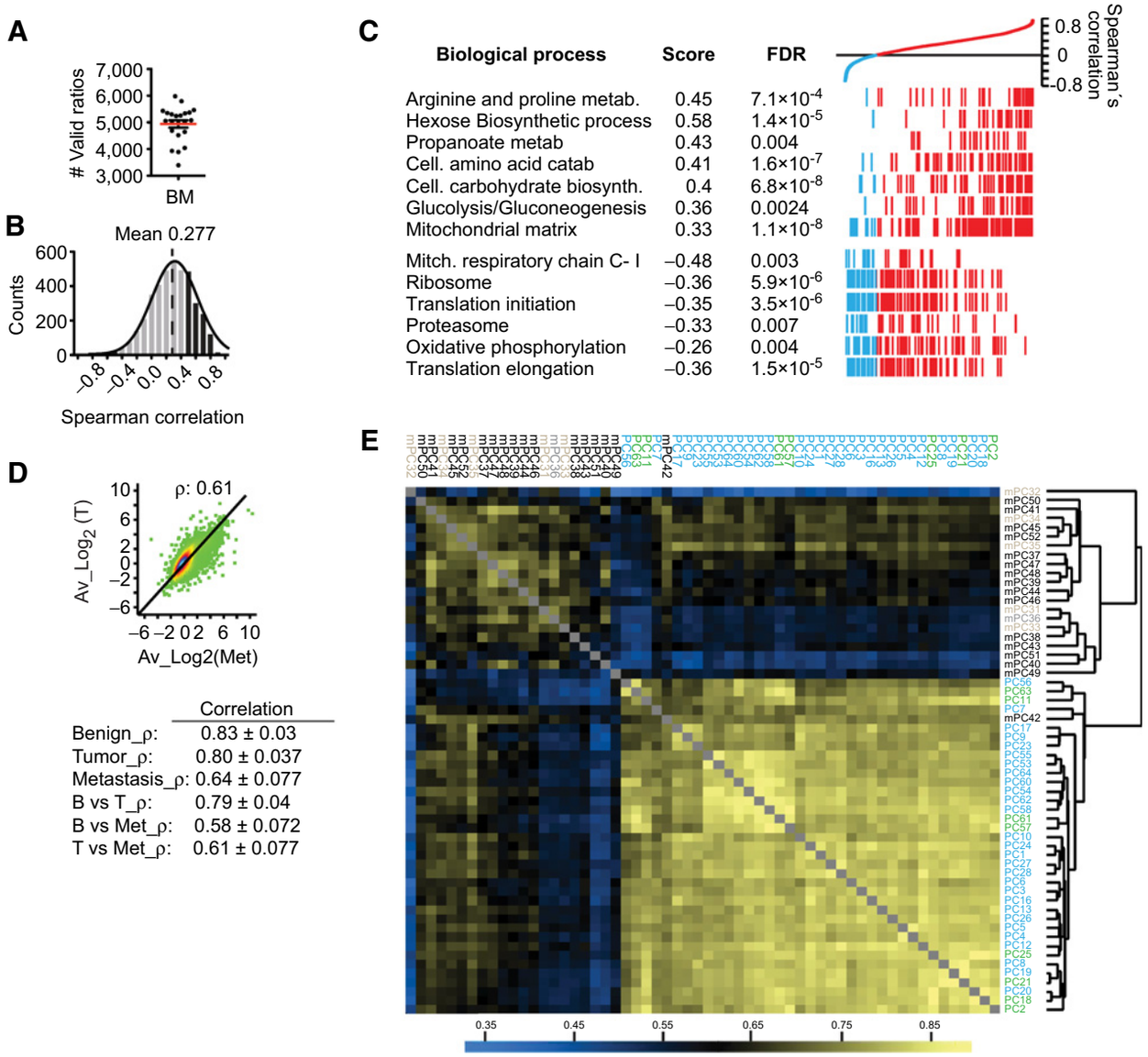

Figure 1.

Proteomic profile of bone metastasis prostate cancer. **A,** Number of valid SILAC ratios obtained per prostate cancer bone metastatic tumor. **B,** Spearman correlation between protein and mRNA expression variation pairs obtained from the same tumor sample. Black bars indicate correlation with $P < 0.05$. **C,** Biological processes with generally high and low correlation between protein and mRNA expression based on the variation of their components (see Materials and Methods section). **D,** Scatter plot of the average protein expression in localized prostate tumors (T) compared with prostate cancer bone metastases (Met). Color represents density. **E,** Hierarchical cluster of localized prostate tumors (blue), neighboring benign prostate tissue (green), and prostate cancer bone metastases (black, castration-resistant tumors; brown, hormone-naïve tumors; gray, tumor collected shortly after the beginning of the androgen-deprivation therapy).

in RNA biogenesis and transport, lipid transport, and fatty acid oxidation (Fig. 2A). Strikingly, these general features of bone metastases were observed regardless of whether the patients were previously subjected to ADT or presented as treatment-naïve cases. This suggests that transition from localized to metastatic spreading requires the acquisition of aggressive features that are retained or further developed when relapsing after castration. It also supports the notion that castration-resistant metastases rely on similar mechanisms (including AR-regulated pathways) for growth as advanced, castration-naïve tumors.

Proteomic subtyping of prostate cancer bone metastases based on an inverse relation between proliferation and metabolic features

High proliferation rate is a general feature of metastatic tumors, and in this study, increased expression of cell-cycle–associated proteins was also highlighted when comparing the proteomes of metastatic and localized prostate cancer. However, given the variability in protein expression among metastases, we set out to analyze whether subgroups of bone metastases existed based on differential expression of cell-cycle–regulating proteins. As a

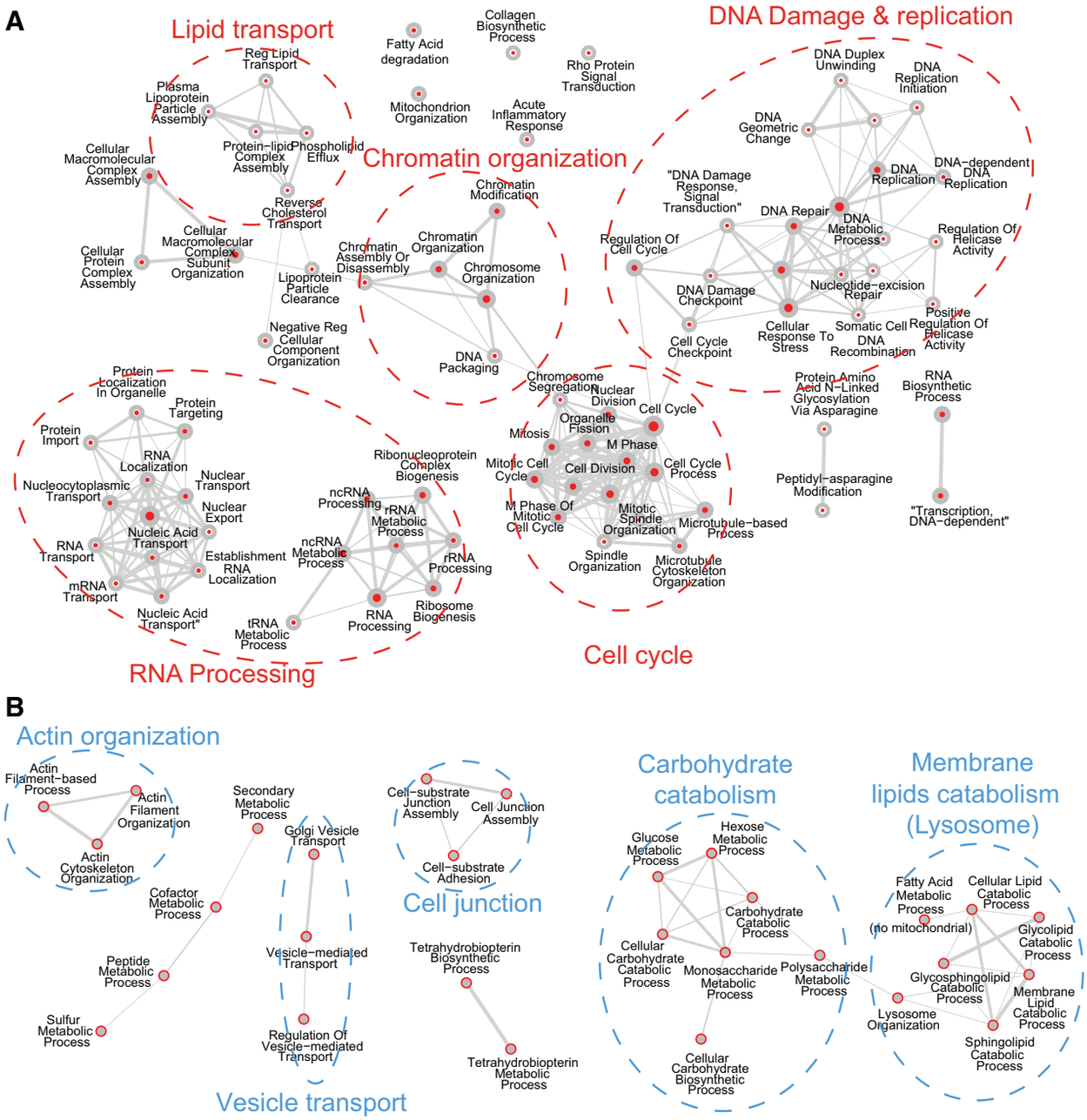

Figure 2.

Network representation of gene ontology terms enriched among proteins differentially regulated between localized and metastatic prostate cancer tumors. Functional categories overrepresented among the proteins with elevated (**A,** red) or reduced (**B,** blue) expression in the bone metastasis compared with localized tumors. Categorical enrichment was calculated using DAVID and enrichment results were plotted using Cytoscape. Line thickness represents number of shared proteins between categories. On each node, the size of the red inner circle and the thickness of the red ring relates to the number of proteins upregulated and downregulated, respectively.

proxy for the proliferation rate, we analyzed expression levels of the MCM complex, a DNA helicase with an essential role in licensing DNA replication origin in the early S-phase of the cell cycle (23). Tumors with higher expression of MCM proteins are predicted to contain more cells in an actively replicative state. The expression levels of the six core proteins of the complex (MCM2-7, ref. 23) showed a high degree of intrasample correlation across the tumors tested ($\rho > 0.895$; Supplementary Fig. S2). Moreover, the expression of the MCM complex remained stable across the localized tumors but varied widely across the bone metastases (Fig. 3A; Supplementary Fig. S2), suggesting variable proliferation rates among metastatic tumors. We then correlated the average

expression of the MCM proteins with all the proteins identified that showed at least two thirds of valid expression ratios across all metastatic samples analyzed. Proteins showing expression levels that significantly ($P < 0.05$) correlated to those of the MCM complex were grouped as positive or negative correlators, respectively (Fig. 3A). As expected, the biological functions among the 240 proteins that positively correlated with MCM expression (Supplementary Table S2) were mainly related to cell-cycle progression, DNA metabolism (i.e., DNA replication and DNA damage repair), and RNA metabolism (including RNA splicing; Fig. 3B), but surprisingly did not contain the widely used proliferation marker, Ki67 ($\rho = 0.37$; $P > 0.05$). On the other hand, the 260 proteins that negatively correlated to the MCM complex were enriched for proteins involved in metabolic functions such as mitochondrial respiration (e.g., COX and NDUF proteins), fatty acid β-oxidation and amino acid catabolism (e.g., ACAD9, ACADSB, and IVD), and Golgi-ER organization (e.g., COGs and COPA; Fig. 3B; Supplementary Table S2). Interestingly, this group was also enriched for proteins positively regulated via the canonical AR pathway (e.g., PSA, STEAP2, AGR2, GDF15, FASN, PDIA5, CORO2a, and NT5DC3; refs. 20, 24, 25). Our results suggest that metastatic tumors with slower proliferation rates preferentially rely on aerobic metabolism for energy production, while the enlarged Golgi-ER compartment of these tumors could reflect a secretory function as a sign of somewhat retained prostate epithelial differentiation. Interestingly, these metabolic and secretory features are characteristics of tumors localized to the prostate, which are in general also characterized by a low proliferation rate (13).

To further support these observations, we compared these two sets of proteins (positively and negatively correlated to the MCM proteins, respectively) with independent system-wide transcriptomic studies of prostate cancer using GSEA (17). As anticipated, the mRNA levels corresponding to proteins positively correlated with the MCM complex were typically elevated in metastatic compared with localized prostate tumors (Supplementary Fig. S3A; refs. 9, 26; and this study). On the other hand, negatively correlated proteins showed overall reduced expression in metastases relative to localized prostate cancer (Supplementary Fig. S3B; refs. 9, 26; and this study), while being genes with increased expression at early stages (i.e., in localize tumors as compared with benign prostate tissue; Supplementary Fig. S3C; refs. 9, 13, 26). This suggests that metastases with predominant expression of proteins negatively correlated with the MCM complex retain features of localized tumors with low proliferation rates and would potentially show a less aggressive phenotype. We next used hierarchical clustering to analyze whether the protein signature defined through correlation to the MCM complex could serve to identify subgroups of metastatic tumors. Indeed, using this protein signature, tumors could be grouped in two main clusters (BM1 and BM2; Fig. 4A), which contained all but three of the tumors (sample PC32 was excluded from the analysis due to large percentage of missing values). A direct comparative analysis of the tumors included on each of the clusters showed indeed that BM1 metastases express significantly higher levels of mitochondrial and ER/Golgi proteins typical of localized tumors, while proteins with increased expression in BM2 tumors are enriched in proliferation-related processes (DNA replication, mitosis, and mRNA processing; Fig. 4B). Taken together, these results suggest the existence of at least two subtypes of bone metastases; one (BM1), including tumors that retain features of differentiated prostate epithelium, with potentially less aggressive phenotype; and another (BM2), grouping highly proliferative and less-differentiated metastases.

We further validated the presence of these phenotypic subgroups by IHC analysis of an extended cohort of 65 prostate cancer bone metastases. Immunoreactivity of PSA, as secretion marker related to prostate epithelial cell differentiation and representative of group BM1, and nuclear MCM3, as marker of proliferation and representative of the BM2 group, was assessed (Supplementary Fig. S4A). In good agreement with the proteomic data (PSA/MCM3 correlation $\rho = -0.77$; $P < 0.0001$; $n = 22$), the fraction of MCM3 immuno-positive tumor cells was inversely correlated to the PSA immunoreactivity ($\rho = -0.58$; $P < 0.0001$; $n = 65$; Fig. 4C). Metastases with MCM3 scores at or below median (≤ 21) and PSA scores above the median (>6) could be considered as BM1-like, while metastases with MCM3 scores above 21, and PSA scores at or below 6 are more likely BM2-like. Tumors clustered as part of one of these groups composed two thirds of the cohort analyzed, while the rest showed a heterogeneous phenotype in relation to these two markers as observed in Supplementary Fig. S4A.

Increased expression of proliferation markers in primary prostate tumors is correlated with poorer prognosis (27) and commercial test are available to evaluate these features (e.g., Prolaris). In order to investigate whether the observed proliferation features of BM2 tumors were present in the primary tumors or were instead acquired at a later stage, we analyzed MCM3 and PSA expression in diagnostic biopsies corresponding to 12 and 14, respectively, of our proteomic analyzed metastases. On the one hand, MCM3 levels were similar in primary biopsies independently of whether the consequent metastasis showed features of the BM1 or BM2 phenotypic subgroups (Fig. 4D), but importantly they were increased in bone metastases compared with paired diagnostic biopsies ($P = 0.010$, $n = 12$) and the increase seemed more pronounced in BM2 than BM1 metastases (Fig. 4D). On the other hand, levels of PSA on biopsies from tumors that developed into BM2 metastases were lower than those resulting in BM1 metastases ($P = 0.023$, $n = 12$), and PSA levels were further decreased in metastases compared with diagnostic biopsies ($P = 0.030$, $n = 14$; Fig. 4E).

Taken together, the IHC analysis confirmed the proteomic data showing that prostate cancer bone metastatic progression is associated with increased proliferation, and suggests that early loss of AR canonical function drives a separate path of metastatic development upon castration treatment.

Phenotypic subtypes of prostate cancer bone metastases correlate with disease outcome and could provide bases for therapeutic stratification of patients

According to the protein profiles of tumors obtained from castration-naïve and castration-resistant patients, the bone metastasis phenotypes seemed to be independent from previous treatment (Fig. 4A; Supplementary Fig. S3C). Instead, the large variation in MCM3-positive tumor cells (3%–94%) and PSA immune score (0–12) appeared to be related to patient prognosis. Patients with BM2-like metastases (as defined above, $n = 22$) had shorter survival times after first ADT compared with the BM1-like group ($n = 21$; median survival 30 vs. 68 months, log-rank = 4.6, $P = 0.032$, Fig. 5A). Moreover, when the survival of BM2-like patients was compared with the rest of the cohort ($n = 43$), the survival time after first ADT was significantly reduced (median survival 30 vs. 46 months, log-

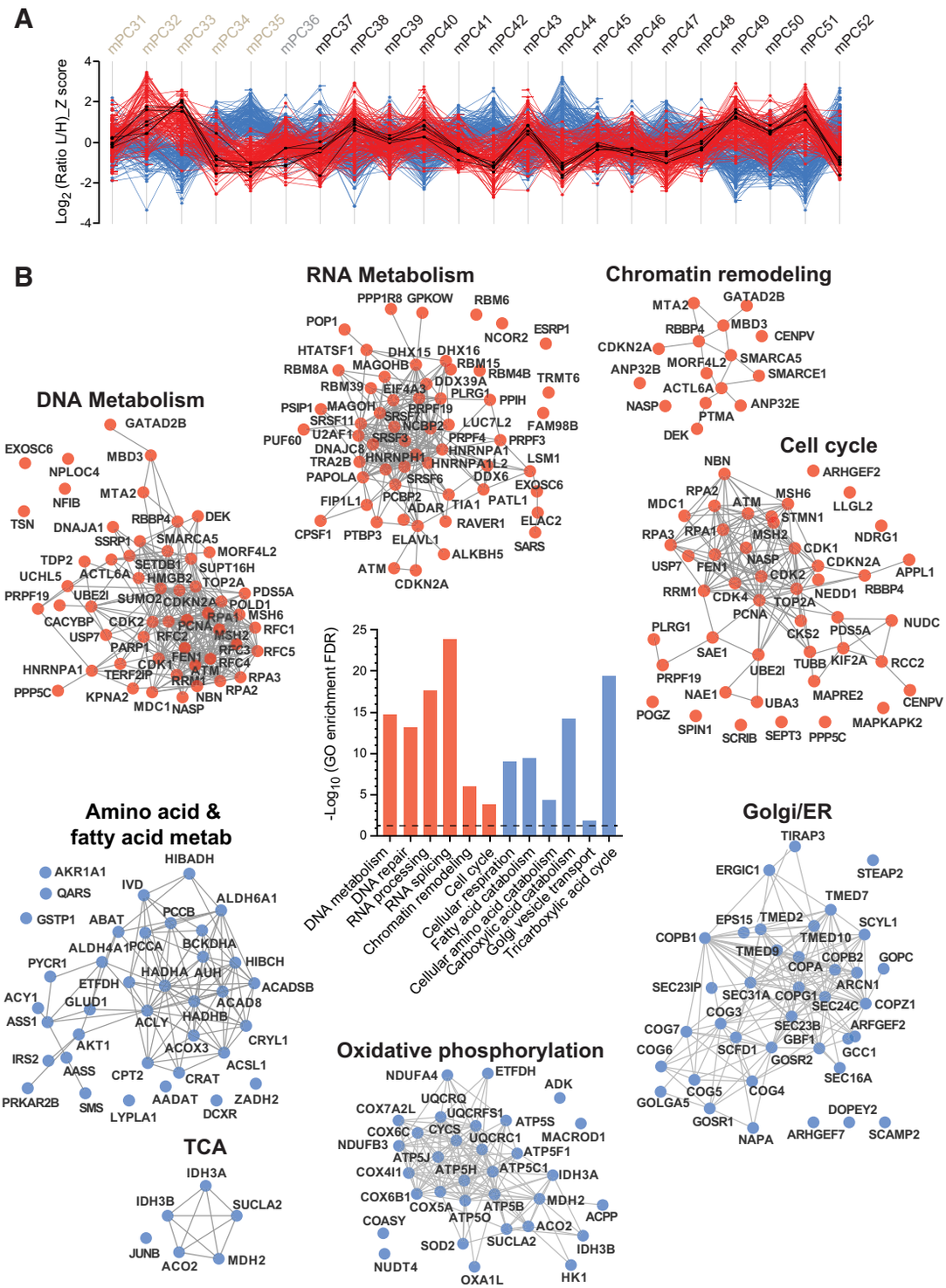

Figure 3.

Set of proteins that positively or negatively correlate with the expression of the MCM complex. **A,** The protein expression profile across metastatic tumors of MCM complex protein components was set as reference (black lines). Expression profiles of proteins that positively and negatively correlated with the average expression of the MCM proteins are presented in red and blue, respectively. Profile shows the expression as $\log_2$ of the SILAC intensity ratio for each protein after application of Z-transformation. Tumors: brown (mPC31-35), hormone-naïve tumors; black (mPC37-52), castration-resistant tumors; gray (mPC36), tumor collected shortly after the beginning of the androgen-deprivation therapy. **B,** Functional categories overrepresented among the proteins that positively (red) and negatively (blue) correlate with the average expression of the MCM complex components. Network representation of the proteins of each category was displayed according to the String database score and plotted using Cytoscape (www.string-db.org; ref. 16).

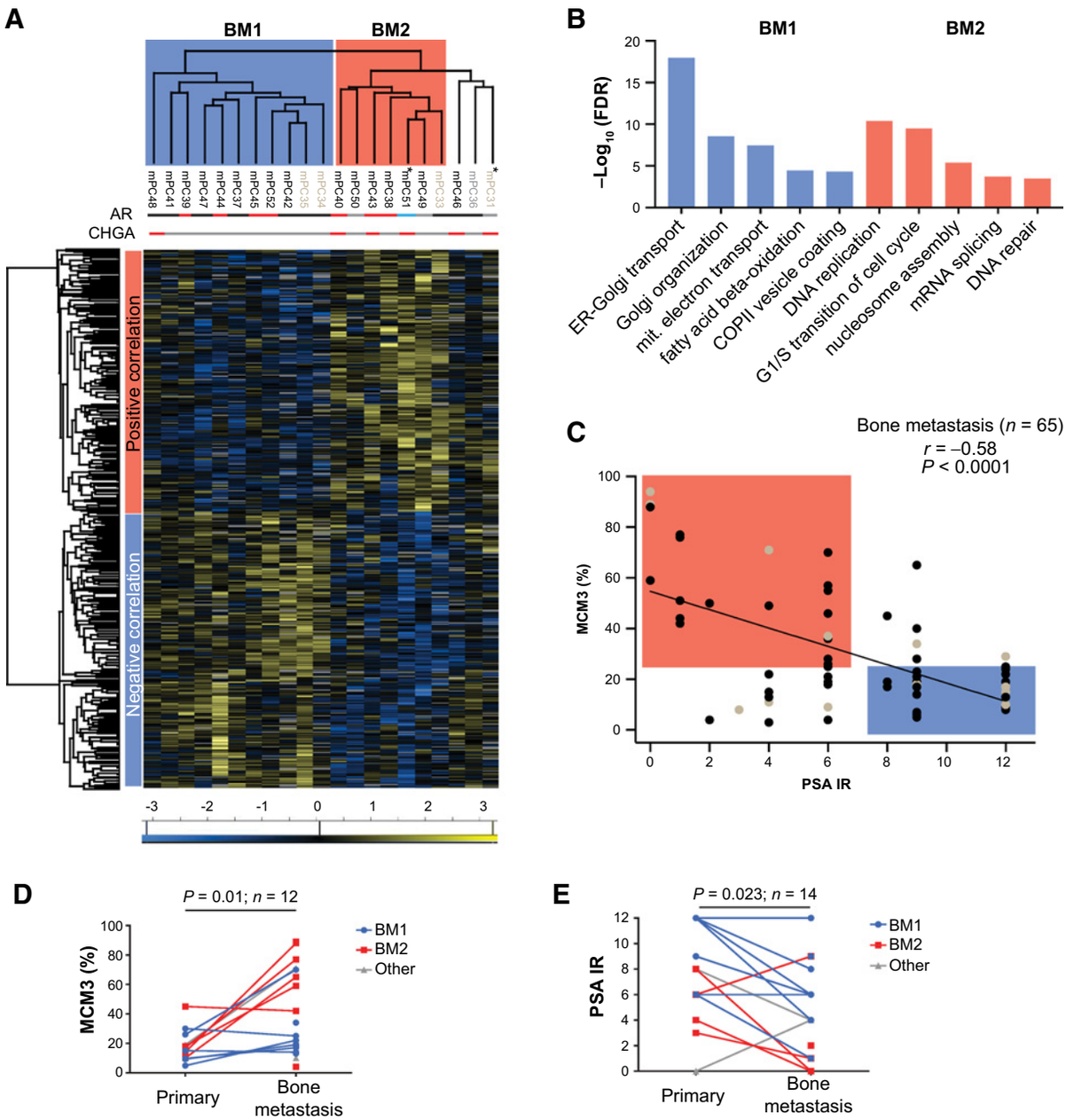

Figure 4.

Phenotypic subgroups of prostate cancer bone metastasis. **A,** Hierarchical clustering of prostate cancer bone metastatic tumors (mPC31-52) according to the expression of the selected proteins that significantly correlate (positively or negatively) with the expression of the MCM complex, resulting in two main clusters; BM1 and BM2. AR and CHGA expression is indicated. Gray represents protein not detected in the sample; blue, expression lower than the mean in localized tumors minus 2 standard deviations; red, expression higher than the mean in localized tumors plus 2 standard deviations; black, similar levels as in localized tumors. For CHGA, red indicates protein being detected and quantified. *, Tumors with canonical neuroendocrine features of low AR and high CHGA expression as addressed by IHC. **B,** Gene ontology of the biological processes and cellular compartments enriched among the proteins significantly upregulated ($P < 0.05$; fold change, 1.5) in BM1 compared with BM2 metastases (blue) and vice versa (red). The Y axis indicates the $-\log_{10}$ (FDR of the enrichment). **C,** Correlation between the immunoreactivity of MCM3 and PSA in each tumor of the validation cohort. **D** and **E,** MCM3 (**D**) and PSA (**E**) immunoreactivity was evaluated on diagnostic biopsies and paired prostate cancer bone metastasis. Color represents the metastatic subgroup of each patient.

rank = 5.7, $P = 0.017$, Fig. 5B). Importantly, the combined immuno-variable defining BM2-like metastases (MCM3 fraction above median and PSA IR below median) added prognostic value to either MCM3 or PSA immunoreactivity analyzed as single variables (Supplementary Table S3), also when adjusted for age and Gleason score at diagnosis. In contrast, neither of the clinical variables in Table 1 was significantly associated with survival after first ADT (Supplementary Table S3).

In addition to a possible difference in prognosis, the distinct phenotypic characteristics of the two metastasis subtypes could be of importance for patient stratification into different treatments. Despite the lack of cell line models accurately resembling all the phenotypic features of each subgroup, we tested, as proof of principle, whether cell sensitivity toward cellular organelle poisoning was related to the amount of organelle per cell. Thus, C4-2b cells with proportionally more mitochondrial content were more sensitive to drugs targeting mitochondrial function (metformin and doxycycline; Supplementary Fig. S4B). On the other hand, PC3 cells, with enlarged Golgi compartment, were more sensitive to brefeldin A treatment, a drug that interferes with ER to Golgi transport (Supplementary Fig. S4B).

Discussion

In this study, we have performed an extensive characterization of the prostate cancer bone metastasis proteome, as the bone is the preferred metastasis niche for advanced prostate cancer. Surgical removal of bone metastases is seldom performed and, therefore, most studies of prostate cancer metastases so far have been based on soft-tissue metastases obtained from rapid autopsy programs and include patients with exhausted treatment options (28). In contrast, our study cohort was mainly composed of chemotherapy-naïve bone metastases and even included cases obtained prior to any therapy. The analysis of those valuable metastasis samples, in combination with data from our previous study of the primary prostate cancer proteome (13), allowed us to describe prostate cancer evolution at the proteome level for the first time. This revealed the existence of two phenotypically distinct subtypes of prostate cancer bone metastasis, which are related to disease prognosis and may have implications for future personalized treatments. Limitations of this study include the limited number of samples analyzed and the unavailability of an independent replication cohort. A separate analysis of the epithelial and stromal components could provide additional information regarding the relative influence of the tumor microenvironment on proteome variation during prostate cancer progression.

The molecular transition from localized to metastatic prostate cancer is not yet well understood. Here, we found that at the proteome level, castration-naïve bone metastases show a proteome pattern distinct from untreated localized prostate cancer but similar to castration-resistant bone metastases. This suggests that metastases growing in the bone and thus influenced by this microenvironment (29) have acquired most features of aggressive tumors, such as accelerated cell-cycle progression, already prior to therapy selection (Fig. 2; ref. 30). Whether acquisition of this aggressive phenotype is a requirement for metastatic spreading or it is achieved upon reaching the metastatic niche remains to be elucidated. The increased activity in signaling pathways related to cell-cycle and DNA damage response in soft-tissue metastases previously reported (10), together with the observed increased expression of MCM3 protein in bone metastasis compared with diagnostic biopsies, suggests that these are features of metastatic prostate cells. Our data also indicate that castration-resistant prostate cancer bone metastases maintain their aggressive growth behavior under the environmental circumstances of low androgen availability, by often but not always restoring canonical AR signaling.

We observed that prostate cancer bone metastases are heterogeneous in their protein repertoire and propose the existence of at least two phenotypically distinct subgroups (Fig. 5). Group BM1, characterized by elevated expression of many canonical AR targets and by higher mitochondrial and ER/Golgi organelle content as indicatives of aerobic metabolism and secretory functions and BM2, defined by increased expression of proteins required for cell-cycle progression and likely driven by glycolytic metabolism. Inverse correlation between AR canonical activity and tumor aggressiveness has been previously suggested for localized prostate cancer (28, 31), but with limited characterization of the metabolic tumor features. The features of BM2 type of metastases are not commonly seen within localized prostate cancer, but importantly, when observed, they are associated with poor patient prognosis (27). On the other hand, features of BM1 tumors are often recognized in early prostate cancer (13), suggesting this group includes tumors with higher degree of epithelial cell differentiation. Whether more differentiated BM1 metastases retain their molecular features throughout the treatment regimen until patient death or if they change as an adaptive mechanism to later therapies deserves further investigation. The use of SILAC spike-in standard from prostate cells ensures quantification accuracy but limits the identification of proteins specific of other cell types within the tumor microenvironment. Therefore, the existence of additional subtypes of prostate cancer bone metastasis, for instance, those exhibiting high degree of immune cells infiltration, cannot be ruled out (10). Whether tumors with high immune cell infiltration constitute and independent subgroup or an additional layer of complexity for the stratification of bone metastasis deserves further investigation. However, taking advantage of some of the bone metastases being analyzed in both this and the Ylitalo and colleagues study (20), tumors with higher degree of immunoreactivity would be of the BM2 type while, as expected, AR-driven tumors are classified as BM1.

The two metastatic phenotypes identified in our study show similarities with molecular subtypes recently suggested for localized prostate tumors based on transcriptomic analysis (31, 32). These studies proposed the existence of three prostate cancer subtypes: two luminal-like (PCS1, PCS2 and luminal A, luminal B, respectively) and one basal-like (PCS3 and basal, respectively). Our BM2 metastases show similarities with the PCS1 and luminal B tumors, being highly proliferative and associated with poor patient prognosis, while our BM1 tumors may have similarities with the PCS2 and luminal A tumors, showing increased canonical AR activity. The PCS3 and basal tumors were not obviously captured by our proteomic approach, probably due to the number of samples analyzed, but may have been reflected as the MCM3 low/PSA low cases by the IHC analysis. The IHC analysis also reflected large intertumoral and intratumoral heterogeneity, with mosaic metastases (areas positive for PSA and negative for MCM3 and vice versa, next to each other) represented in both subgroups (Supplementary Fig. S4A). Tumor heterogeneity may reflect the range of response to secondary treatment, including enzalutamide and abiraterone, observed in the clinic and supports the development of personalized treatments according to the phenotypic features of the tumors (33, 34).

Phenotypic features of prostate cancer bone metastatic tumors seem related to disease prognosis. Patients with high metastasis PSA immunoreactivity (assessed as marker for prostate differentiation) in combination with low proliferation rate appeared to have better prognosis, measured as cancer-specific survival from first ADT treatment. Because the subtypes do not appear to be dependent on first castration treatment, this way of measuring

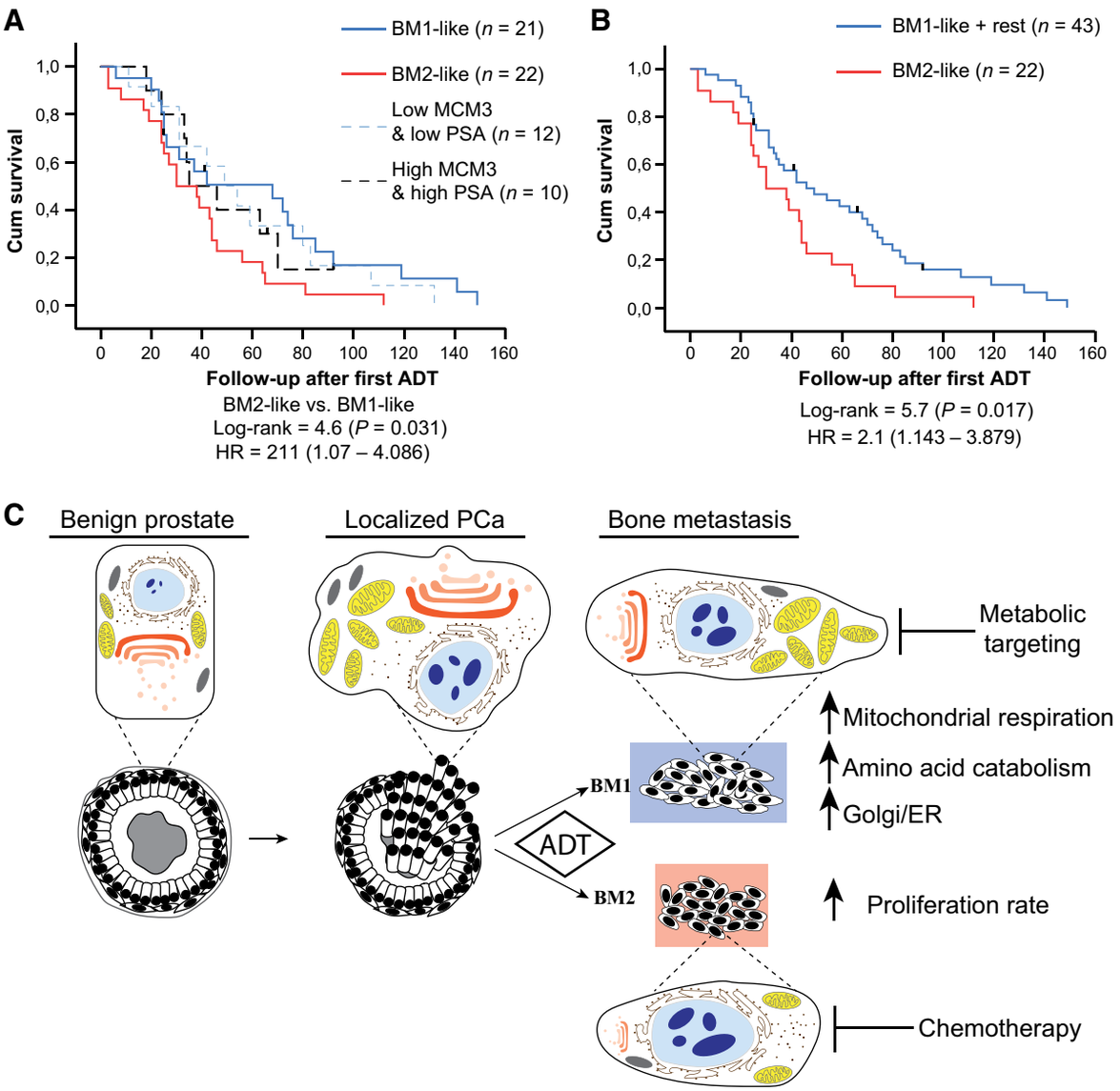

Figure 5.

Phenotypic features of prostate cancer bone metastases show correlation with disease prognosis after first ADT. **A** and **B,** Kaplan–Meier analysis of survival after first ADT of patients bearing prostate cancer bone metastases with different expression of MCM3 and PSA, defined as MCM3 high/low and PSA high/low using median levels (21 and 6, respectively) as cutoffs. **A,** Patients were distributed as their tumors expressed: low MCM3 and high PSA (BM1-like); high MCM3 and low PSA (BM2-like); low MCM3 and low PSA; and high MCM3 and high PSA. **B,** Patients were dichotomized as high MCM3 and low PSA (BM2-like) compared with all other tumors. **C,** Schematic representation of prostate cancer progression model.

survival could reflect the original response to ADT, predicted to be more efficient against BM1, a subgroup clearly AR driven. Interestingly, we were able to detect the expression of neuroendocrine markers such as CHGA by mass spectrometry in a fraction of BM2 tumors (Fig. 4A), in line with the dedifferentiation process and poorer prognosis observed. Of those, only mPC31 and mPC51 could be define as canonical neuroendocrine tumors expressing low AR/PSA levels and high levels of CHGA addressed by IHC (Fig. 4A).

In addition to its relation to prognosis, the existence of phenotypic subgroups might be used for patient stratification for suitable therapeutic options. Thus, BM1 tumors that express higher levels of proteins involved in mitochondrial respiration and secretory functions and maintain canonical AR activity might be sensitive to drugs targeting these metabolic functions (e.g., metformin, doxycycline, or brefeldin A), presumably in combination with AR targeting drugs. This possibility is supported by our *in vitro* data on prostate cancer cells and by previous studies showing that the combination of enzalutamide and metformin treatment in C4-2b cell xenografts reduces tumor volume more effectively than any of the treatments given alone (35). Currently, there are several clinical trials testing the effectiveness of this

combined therapy in patients with CRPC (NCT01677897, NCT01243385, and NCT01796028) but, to the best of our knowledge, no patient selection is being applied based on metabolic or proteomic profiles. Our results suggest that patients with maintained AR activity linked to mitochondrial respiration would benefit the most from this treatment and therefore patient stratification should be considered in future trials.

In an effort to identify drugs that can be repurposed for the treatment of prostate cancer alone or in combination with current treatments, we summarized all approved drugs that target proteins found upregulated in prostate cancer bone metastases compared with prostate localized tumors (Supplementary Fig. S5) and those particularly targeting each of the subgroups (Supplementary Fig. S6). We hope that this overview of current drug targets in the context of prostate cancer progression may serve to motivate clinical studies for drug repurposing or the utilization of novel drug combinations. Indeed, targeting of proteins like mTOR, with functions both in cellular proliferation (RNA metabolism and translation) and energy generation (fatty acid metabolism) is currently being tested in clinical trials in combination with AR targeting therapies (www.clinicaltrial.org; clinical trial IDs NCT02407054 and NCT02091531). Note that some of these drugs have already proven inefficient for the treatment of metastatic prostate cancer (e.g., refs. 36–38) and it would be interesting to determine whether these failures are due to lack of efficacy or due to inappropriate patient selection.

In summary, the analysis of the prostate cancer proteome revealed that while localized to the prostate, most tumors are slowly proliferating and exhibit elevated mitochondrial activity and intracellular vesicle transport, associated with secretion and somewhat retained epithelial cell differentiation. Metastatic tumors are more heterogeneous, showing various levels of AR activity, metabolic profiles, and proliferation rates. We propose the existence of at least two phenotypically different subtypes of prostate cancer bone metastases, where patients with highly proliferative, low differentiated prostate cancer bone metastases (BM2) have worse prognosis and potentially would benefit from receiving early chemotherapy-based treatments targeting cell-cycle progression (Fig. 5C). Patients with more differentiated metastases (BM1) seem to show better response to ADT and probably would benefit from second-line AR targeting therapies and treatments directed toward metabolic pathways (Fig. 5C). The proteome analysis of larger cohorts of prostate cancer metastases is warranted in order to validate and refine group features. Whether metastasis heterogeneity can be predicted from analysis of the primary tumor also deserves further investigation.

Disclosure of Potential Conflicts of Interest

No potential conflicts of interest were disclosed.

Authors' Contributions

Conception and design: D. Iglesias-Gato, A. Bergh, A. Flores-Morales, P. Wikström

Development of methodology: D. Iglesias-Gato, A. Widmark, M. Mann

Acquisition of data (provided animals, acquired and managed patients, provided facilities, etc.): D. Iglesias-Gato, S. Crnalic, T.S. Lima, T. Geiger, A. Widmark, A. Bergh, P. Wikström

Analysis and interpretation of data (e.g., statistical analysis, biostatistics, computational analysis): D. Iglesias-Gato, E. Thysell, S. Tyanova, A. Santos, T.S. Lima, J. Cox, A. Bergh, A. Flores-Morales, P. Wikström

Writing, review, and/or revision of the manuscript: D. Iglesias-Gato, E. Thysell, S. Crnalic, A. Santos, A. Widmark, A. Bergh, A. Flores-Morales, P. Wikström

Administrative, technical, or material support (i.e., reporting or organizing data, constructing databases): D. Iglesias-Gato, S. Crnalic, A. Flores-Morales

Study supervision: D. Iglesias-Gato, A. Flores-Morales

Acknowledgments

The authors are grateful to Pernilla Andersson, Susanne Gidlund, and Igor Paron for excellent technical assistance and acknowledge the Uppsala-Umeå Comprehensive Cancer Consortium for giving access to biobank samples. This work was supported by grants from the Danish Research Council (DFF 4004-00450, Flores-Morales), the Movember Foundation (Flores-Morales), and the Danish Cancer Society (R90-A6060-14-S2, Flores-Morales); Swedish Research Council (K2013-64X-20407-04-3, Wikström), the Swedish Cancer Society (CAN 2016/824, CAN 2013/1324, Wikström and 130293, Bergh), Swedish Foundation for Strategic Research (RB13-0119, Wikström); Swedish Cancer Society (CAN 2015/732 Widmark). The Novo Nordisk Foundation Center for Protein Research, University of Copenhagen is supported financially by the Novo Nordisk Foundation (Grant agreement NNF14CC0001).

The costs of publication of this article were defrayed in part by the payment of page charges. This article must therefore be hereby marked *advertisement* in accordance with 18 U.S.C. Section 1734 solely to indicate this fact.

Received April 20, 2018; revised June 13, 2018; accepted July 18, 2018; published first July 24, 2018.

References

1. Coleman RE. Clinical features of metastatic bone disease and risk of skeletal morbidity. Clin Cancer Res 2006;12(20 Pt 2):6243s–9s.
2. Gandaglia G, Karakiewicz PI, Briganti A, Passoni NM, Schiffmann J, Trudeau V, et al. Impact of the site of metastases on survival in patients with metastatic prostate cancer. Eur Urol 2015;68:325–34.
3. Parker C, Gillessen S, Heidenreich A, Horwich A, Committee EG. Cancer of the prostate: ESMO Clinical Practice Guidelines for diagnosis, treatment and follow-up. Ann Oncol 2015;26Suppl 5:v69–77.
4. Nuhn P, De Bono JS, Fizazi K, Freedland SJ, Grilli M, Kantoff PW, et al. Update on systemic prostate cancer therapies: management of metastatic castration-resistant prostate cancer in the era of precision oncology. Eur Urol 2018.doi 10.1016/j.eururo.2018.03.028.
5. Barbosa PV, Thomas IC, Srinivas S, Buyyounouski MK, Chung BI, Chertow GM, et al. Overall survival in patients with localized prostate cancer in the US Veterans Health Administration: Is PIVOT Generalizable? Eur Urol 2016;70:227–30.
6. Wilt TJ, Brawer MK, Jones KM, Barry MJ, Aronson WJ, Fox S, et al. Radical prostatectomy versus observation for localized prostate cancer. N Engl J Med 2012;367:203–13.
7. Cancer Genome Atlas Research N. The molecular taxonomy of primary prostate cancer. Cell 2015;163:1011–25.
8. Robinson D, Van Allen EM, Wu YM, Schultz N, Lonigro RJ, Mosquera JM, et al. Integrative clinical genomics of advanced prostate cancer. Cell 2015;162:454.
9. Grasso CS, Wu YM, Robinson DR, Cao X, Dhanasekaran SM, Khan AP, et al. The mutational landscape of lethal castration-resistant prostate cancer. Nature 2012;487:239–43.
10. Drake JM, Paull EO, Graham NA, Lee JK, Smith BA, Titz B, et al. Phosphoproteome integration reveals patient-specific networks in prostate cancer. Cell 2016;166:1041–54.
11. Schwanhausser B, Busse D, Li N, Dittmar G, Schuchhardt J, Wolf J, et al. Global quantification of mammalian gene expression control. Nature 2011;473:337–42.
12. Zhang B, Wang J, Wang X, Zhu J, Liu Q, Shi Z, et al. Proteogenomic characterization of human colon and rectal cancer. Nature 2014;513:382–7.
13. Iglesias-Gato D, Wikstrom P, Tyanova S, Lavallee C, Thysell E, Carlsson J, et al. The proteome of primary prostate cancer. Eur Urol 2016;69:942–52.

14. Huang da W, Sherman BT, Stephens R, Baseler MW, Lane HC, Lempicki RA. DAVID gene ID conversion tool. Bioinformation 2008;2:428–30.
15. Cline MS, Smoot M, Cerami E, Kuchinsky A, Landys N, Workman C, et al. Integration of biological networks and gene expression data using Cytoscape. Nat Protoc 2007;2:2366–82.
16. Szklarczyk D, Morris JH, Cook H, Kuhn M, Wyder S, Simonovic M, et al. The STRING database in 2017: quality-controlled protein-protein association networks, made broadly accessible. Nucleic Acids Res 2017;45:D362–8.
17. Subramanian A, Tamayo P, Mootha VK, Mukherjee S, Ebert BL, Gillette MA, et al. Gene set enrichment analysis: a knowledge-based approach for interpreting genome-wide expression profiles. Proc Natl Acad Sci U S A 2005;102:15545–50.
18. Cox J, Hein MY, Luber CA, Paron I, Nagaraj N, Mann M. Accurate proteome-wide label-free quantification by delayed normalization and maximal peptide ratio extraction, termed MaxLFQ. Mol Cell Proteomics 2014;13:2513–26.
19. Hornberg E, Ylitalo EB, Crnalic S, Antti H, Stattin P, Widmark A, et al. Expression of androgen receptor splice variants in prostate cancer bone metastases is associated with castration-resistance and short survival. PLoS One 2011;6:e19059.
20. Ylitalo EB, Thysell E, Jernberg E, Lundholm M, Crnalic S, Egevad L, et al. Subgroups of castration-resistant prostate cancer bone metastases defined through an inverse relationship between androgen receptor activity and immune response. Eur Urol 2017;71:776–87.
21. Chen G, Gharib TG, Huang CC, Taylor JM, Misek DE, Kardia SL, et al. Discordant protein and mRNA expression in lung adenocarcinomas. Mol Cell Proteomics 2002;1:304–13.
22. Latonen L, Afyounian E, Jylha A, Nattinen J, Aapola U, Annala M, et al. Integrative proteomics in prostate cancer uncovers robustness against genomic and transcriptomic aberrations during disease progression. Nat Commun 2018;9:1176.
23. Li N, Zhai Y, Zhang Y, Li W, Yang M, Lei J, et al. Structure of the eukaryotic MCM complex at 3.8 A. Nature 2015;524:186–91.
24. Cai C, Wang H, Xu Y, Chen S, Balk SP. Reactivation of androgen receptor-regulated TMPRSS2:ERG gene expression in castration-resistant prostate cancer. Cancer Res 2009;69:6027–32.
25. Sharma NL, Massie CE, Ramos-Montoya A, Zecchini V, Scott HE, Lamb AD, et al. The androgen receptor induces a distinct transcriptional program in castration-resistant prostate cancer in man. Cancer Cell 2013;23:35–47.
26. Taylor BS, Schultz N, Hieronymus H, Gopalan A, Xiao Y, Carver BS, et al. Integrative genomic profiling of human prostate cancer. Cancer Cell 2010;18:11–22.
27. Cuzick J, Swanson GP, Fisher G, Brothman AR, Berney DM, Reid JE, et al. Prognostic value of an RNA expression signature derived from cell cycle proliferation genes in patients with prostate cancer: a retrospective study. Lancet Oncol 2011;12:245–55.
28. Kumar A, Coleman I, Morrissey C, Zhang X, True LD, Gulati R, et al. Substantial interindividual and limited intraindividual genomic diversity among tumors from men with metastatic prostate cancer. Nat Med 2016;22:369–78.
29. Bergstrom SH, Rudolfsson SH, Bergh A. Rat prostate tumor cells progress in the bone microenvironment to a highly aggressive phenotype. Neoplasia 2016;18:152–61.
30. Tomlins SA, Mehra R, Rhodes DR, Cao X, Wang L, Dhanasekaran SM, et al. Integrative molecular concept modeling of prostate cancer progression. Nat Genet 2007;39:41–51.
31. You S, Knudsen BS, Erho N, Alshalalfa M, Takhar M, Al-Deen Ashab H, et al. Integrated classification of prostate cancer reveals a novel luminal subtype with poor outcome. Cancer Res 2016;76:4948–58.
32. Zhao SG, Chang SL, Erho N, Yu M, Lehrer J, Alshalalfa M, et al. Associations of luminal and basal subtyping of prostate cancer with prognosis and response to androgen deprivation therapy. JAMA Oncol 2017;3:1663–72.
33. Beer TM, Armstrong AJ, Rathkopf D, Loriot Y, Sternberg CN, Higano CS, et al. Enzalutamide in men with chemotherapy-naive metastatic castration-resistant prostate cancer: extended analysis of the phase 3 PREVAIL study. Eur Urol 2017;71:151–4.
34. Ryan CJ, Smith MR, de Bono JS, Molina A, Logothetis CJ, de Souza P, et al. Abiraterone in metastatic prostate cancer without previous chemotherapy. N Engl J Med 2013;368:138–48.
35. Nguyen HG, Yang JC, Kung HJ, Shi XB, Tilki D, Lara PN Jr, et al. Targeting autophagy overcomes Enzalutamide resistance in castration-resistant prostate cancer cells and improves therapeutic response in a xenograft model. Oncogene 2014;33:4521–30.
36. Araujo JC, Trudel GC, Saad F, Armstrong AJ, Yu EY, Bellmunt J, et al. Docetaxel and dasatinib or placebo in men with metastatic castration-resistant prostate cancer (READY): a randomised, double-blind phase 3 trial. Lancet Oncol 2013;14:1307–16.
37. Michaelson MD, Oudard S, Ou YC, Sengelov L, Saad F, Houede N, et al. Randomized, placebo-controlled, phase III trial of sunitinib plus prednisone versus prednisone alone in progressive, metastatic, castration-resistant prostate cancer. J Clin Oncol 2014;32:76–82.
38. Smith M, De Bono J, Sternberg C, Le Moulec S, Oudard S, De Giorgi U, et al. Phase III study of cabozantinib in previously treated metastatic castration-resistant prostate cancer: COMET-1. J Clin Oncol 2016;34:3005–13.